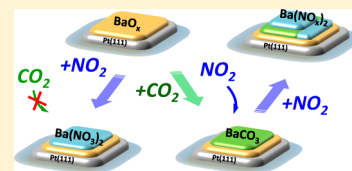


Interactive Surface Chemistry of CO₂ and NO₂ on Metal Oxide Surfaces: Competition for Catalytic Adsorption Sites and Reactivity

Evgeny I. Vovk,^{†,‡} Abdurrahman Turksoy,[†] Valerii I. Bukhtiyarov,[‡] and Emrah Ozensoy^{*,†}[†]Chemistry Department, Bilkent University, 06800 Bilkent, Ankara, Turkey[‡]Boreskov Institute of Catalysis, 630090 Novosibirsk, Russian Federation

ABSTRACT: Interactive surface chemistry of CO₂ and NO₂ on BaO_x/Pt(111) model catalyst surfaces were investigated via X-ray photoelectron spectroscopy (XPS) and temperature-programmed desorption (TPD) techniques with a particular emphasis on the competition between different adsorbates for the catalytic adsorption sites and adsorbate-induced morphological changes. After NO₂ adsorption, nitrated BaO_x/Pt(111) surfaces do not reveal available adsorption sites for CO₂ at 323 K, irrespective of the presence/absence of exposed Pt sites on the surface. Although NO₂ adsorption on thick BaO_x(>10MLE)/Pt(111) overlayers at 323 K leads to the formation of predominantly nitrate species, NO₂ adsorption on the corresponding carbonated surface leads to the formation of coexisting nitrates and nitrites. The presence of carbonates on BaO_x/Pt(111) overlayers does not prevent NO₂ uptake. Carbonated BaO_x(1.5 MLE)/Pt(111) surfaces (with exposed Pt sites) obtained via CO₂ adsorption can also further interact with NO₂, forming surface nitrate/nitrite species, accompanied by the transformation of surface carbonates into bulk carbonate species. These results suggest that the nitrate formation process requires the presence of two adjacent unoccupied adsorption sites. It is apparent that in the presence of both NO₂ and CO₂, carbonate species formed on Lewis base (O²⁻) sites enable the formation of nitrites on Lewis acid (Ba²⁺) sites. Thermal aging, nitration, and carbonation have a direct impact on the morphology of the two-/three-dimensional (2D/3D) BaO_x aggregates on Pt(111). While thermal aging in vacuum leads to the sintering of the BaO_x domains, nitration and carbonation results in redispersion and spreading of the BaO_x domains on the Pt(111) substrate.



INTRODUCTION

Most of the heterogeneous catalytic reactions rely on the consecutive or simultaneous adsorption of reactants on the catalytically active sites for the generation of products. Along these lines, it is not uncommon for reactants, intermediates, and/or products bearing similar chemical structures to compete for similar catalytically active adsorption sites in heterogeneous catalytic processes. Thus, molecular level understanding of the competition phenomena occurring during the adsorption of reactants/intermediates/products on surfaces is a fundamentally crucial aspect for the elucidation of heterogeneous catalytic reaction mechanisms. Automotive exhaust emission catalysts are not an exception to this subject, where multiple catalytic pathways proceed in a parallel fashion in the presence of a large variety of reactants/intermediates/products. For instance, during the operation of the NO_x storage-reduction (NSR) catalysts,^{1,2} oxygen-rich exhaust gases of lean burn engines are treated in two different alternating operational cycles called lean (abundant in oxygen) and rich (abundant in hydrocarbon) cycles, where toxic NO_x gases are initially oxidized/trapped in the solid state and then successively reduced to harmless N₂.

Despite considerable research efforts, the mechanistic details of the NO_x storage and release processes in NSR catalysis are not yet clear.^{3,4} Under technical operating conditions, NSR processes are strongly influenced by the CO₂ and H₂O species that are present in the exhaust stream. CO₂ and H₂O may directly interact with the NO_x storage material (i.e., BaO) and form BaCO₃ and Ba(OH)₂ species, respectively.^{5,6} Further-

more, the presence of CO₂ in the exhaust stream during the lean cycle was found to decrease the NO_x storage capacity (NSC) of NSR catalysts.^{3,7} It was suggested that the attenuation of the NSC in the presence of CO₂ is associated with the competition between NO₂ and CO₂ species for similar adsorption sites on the NO_x storage domains.^{5,8}

In a former study, thermodynamic calculations were performed on bulk materials in order to estimate the relative stabilities of carbonate and nitrate species on baria.^{6,8} Using such an approach, Rodrigues et al.⁸ reported that at elevated temperatures, bulk BaCO₃ becomes more stable than bulk Ba(NO₃)₂. Along these lines, it was argued that bulk Ba(NO₃)₂ could not be formed through the interaction of NO_x(g) with bulk BaCO₃ under operational conditions. On the other hand, density functional theory (DFT) calculations associated with NO₂ and CO₂ adsorption on the BaO(100)⁹ and BaCO₃(110)¹⁰ surfaces revealed that, although the adsorption strength of CO₂ is higher than that of NO₂ on BaO(100),⁹ NO₂ adsorption on the BaCO₃(110) surface should not be excluded.¹⁰

On the BaO(100) surface, CO₂ was reported to adsorb exclusively on the Lewis base (i.e., O²⁻) sites forming surface carbonates,⁹ while on the stoichiometric BaCO₃(110) surface, CO₂ was reported to adsorb also on the Lewis acid sites (i.e.,

Received: January 28, 2013

Revised: March 13, 2013

Published: March 13, 2013

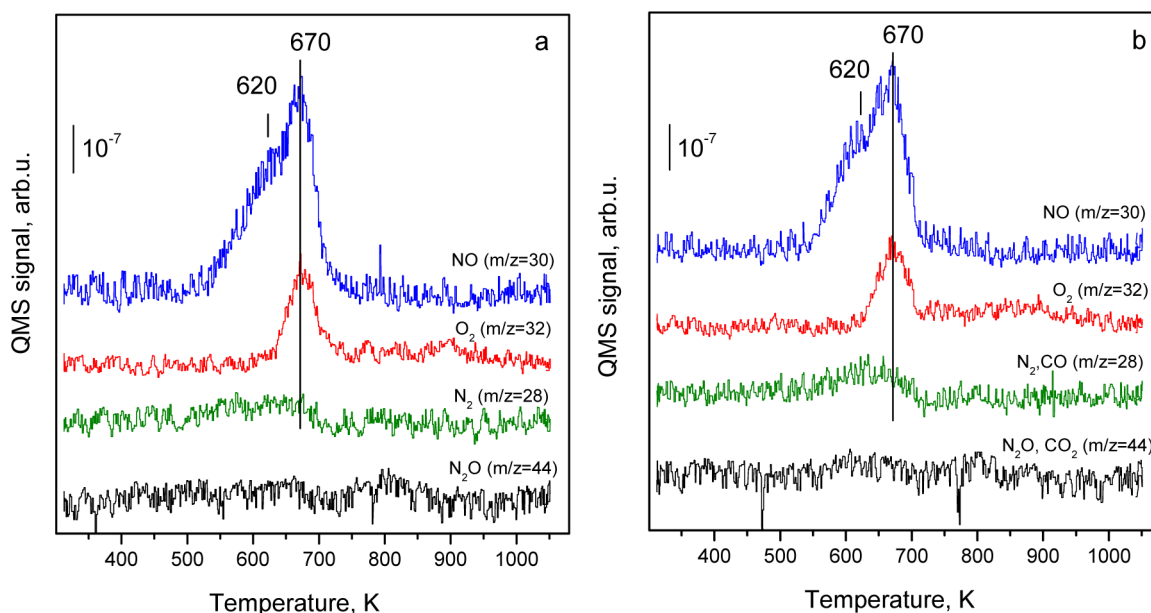


Figure 1. (a) TPD profiles showing NO ($m/z = 30$), O₂ ($m/z = 32$), N₂/CO ($m/z = 28$), and N₂O/CO₂ ($m/z = 44$) desorption channels obtained after exposing a BaO_x(>10 MLE)/Pt(111) surface to 900 L (5×10^{-7} Torr \times 30 min) NO₂(g) at 323 K. (b) TPD spectra obtained after consequent exposure of the BaO_x(10 MLE)/Pt(111) surface first to 1800 L (10^{-6} Torr \times 30 min) NO₂(g), then to 900 L (5×10^{-7} Torr \times 30 min) CO₂(g).

Ba²⁺).¹⁰ It is important to emphasize that on the BaO(100) surface, CO₂ acts as a typical Lewis acid with a high affinity toward O²⁻ sites, and the interaction is mostly driven by Lewis acid/base chemistry in which O²⁻ lone pair electrons of the BaO(100) surface fill the vacant CO₂ acceptor orbitals.¹¹ On the other hand, NO₂ was reported to interact simultaneously with both Lewis basic sites (O²⁻) as well as Lewis acidic sites (Ba²⁺) on the BaO(100) surface forming nitrate (NO₃⁻) and nitrite (NO₂⁻) pairs, which can interact in a synergistic (cooperative) fashion.¹¹ NO₃⁻ and NO₂⁻ surface species can be formed from a nascent adsorbed NO₂ pair as a result of an intermolecular electron transfer yielding Lewis acidic NO₂⁺ and basic NO₂⁻ adsorbates that have high affinity toward O²⁻ and Ba²⁺ surface sites, respectively.^{11–13} The nitrite formation during the initial stages of NO₂ adsorption over BaO surfaces was confirmed experimentally in various reports^{14,15} where the ratio of nitrate to nitrite species was also found to be close to 1 at low temperatures,¹⁴ confirming the formation of the nitrate–nitrite ion pairs.

Hence, in the current work, we focus our attention on the influence of CO₂ on the NO_x storage and release mechanisms of model NSR catalysts with a particular emphasis on the competition between different adsorbates for the catalytic adsorption sites. Along these lines, BaO_x/Pt(111) planar model catalyst surfaces were investigated as a function of the adsorption sequence, BaO domain morphology and the presence/absence of Pt/BaO interfacial sites. Current results provide a valuable fundamental insight on the operational principles of NSR catalysts that can also be extended further to many other analogous competitive adsorption systems that are ubiquitously exploited in surface science and heterogeneous catalysis.

EXPERIMENTAL SECTION

Experiments were performed in a custom-made multitechnique ultrahigh vacuum (UHV) surface analysis chamber with a base pressure of 2×10^{-10} Torr. The UHV chamber is equipped

with X-ray photoelectron spectroscopy (XPS, Riber Mg/Al Dual anode and Riber Model EA 150 Electron Energy Analyzer), temperature-programmed desorption (TPD, Dycor model DM200 M quadrupole mass spectrometer (QMS)), and custom-made reverse view low-energy electron diffraction (LEED) capabilities. During the TPD experiments, N ($m/z = 14$), H₂O ($m/z = 18$), N₂/CO ($m/z = 28$), NO ($m/z = 30$), O₂ ($m/z = 32$), NCO ($m/z = 42$), N₂O/CO₂ ($m/z = 44$), and NO₂ ($m/z = 46$) were monitored, and the sample was heated using a 1 K/s heating ramp. A Pt(111) single crystal disc (10 mm diameter, 2 mm thickness, both sides atomically polished, MaTeck GmbH) was used as a substrate. The Pt(111) single crystal was mounted on Ta wires, which can be resistively heated up to 1073 K. The sample temperature was monitored via a K-type thermocouple (0.05 mm, Omega) spot-welded on the lateral edge of the crystal. The Pt(111) surface was cleaned by multiple cycles of Ar⁺ sputtering (LK technologies, NGI3000) using an accelerating voltage of 1.5 kV and subsequent annealing at 1073 K in vacuum. The cleanliness of the Pt(111) surface was confirmed by XPS and LEED. BaO_x layers on Pt(111) were prepared by thermal evaporation of Ba(g) from a BaAl₄ alloy (ST2/FR wire, SAES Getters) onto the Pt(111) substrate at room temperature and subsequent annealing in O₂ (99.999% purity, Linde AG, 10^{-6} Torr, 573 K, 15 min). The monolayer equivalent (MLE) coverage of the BaO_x films on the Pt(111) substrate was calculated by utilizing the attenuation of the Pt 4f_{7/2} XPS signal, as described elsewhere.^{16–18} NO₂ gas used in experiments was synthesized through the reaction of NO (99.9% purity, Air Products) with O₂ and purified further by subsequent freeze–thaw–pump cycles. CO₂ gas (Linde AG, Purity 99,999%) was used without further purification.

RESULTS AND DISCUSSION

CO₂ and NO₂ Interactions on Thick BaO_x Overlayers over Pt(111) in the Absence of Exposed Pt Adsorption Sites. During these set of experiments, NO₂ and CO₂

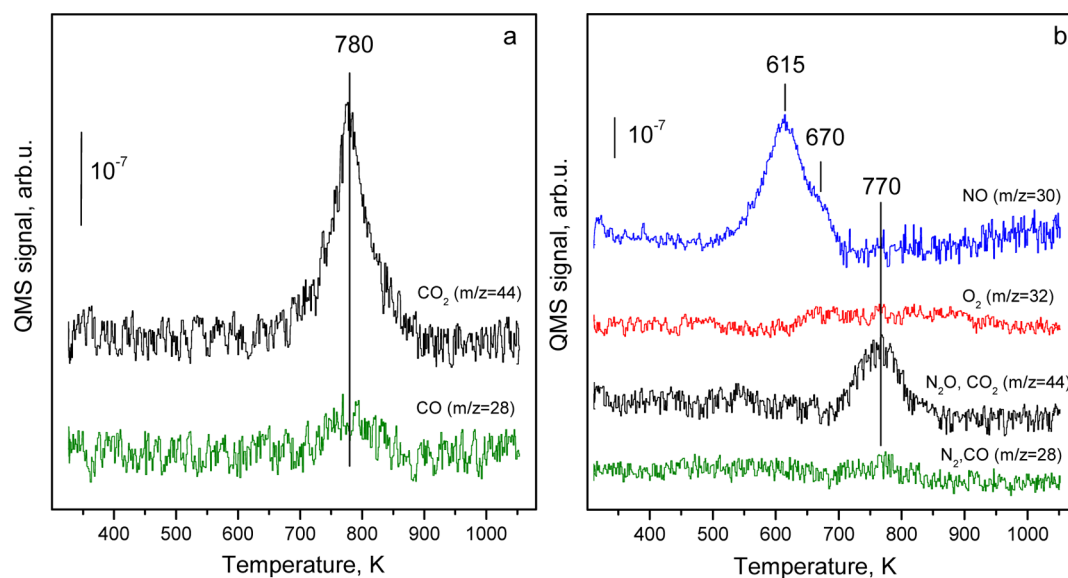


Figure 2. (a) TPD profiles showing NO ($m/z = 30$), O₂ ($m/z = 32$), N₂/CO ($m/z = 28$), and N₂O/CO₂ ($m/z = 44$) desorption channels obtained after exposing a BaO_x(>10 MLE)/Pt(111) surface to 1800 L (10^{-6} Torr \times 30 min) CO₂(g) at 323 K. (b) TPD spectra obtained after consequent exposure of the BaO_x(10 MLE)/Pt(111) surface first to 1800 L (10^{-6} Torr \times 30 min) CO₂(g), then to 1800 L (10^{-6} Torr \times 30 min) NO₂(g).

adsorption were performed on a model catalyst with a relatively thick BaO_x overlayer (i.e., BaO_x(>10 MLE)/Pt(111), which will be referred to as the “thick BaO_x overlayer” hereafter in the text) in order to cover all of the Pt(111) adsorption sites and prevent their direct participation in the gas phase adsorption phenomena. In former studies, it was demonstrated that NO₂ saturation of similar BaO_x overlayers at room temperature resulted in the formation of predominantly nitrate species,^{15,17} in excellent agreement with the currently obtained N1s spectra in XPS, which will be discussed later in the text. The nitrate formation proceeds via nitrite intermediates which were also detected during the initial stages of adsorption. With increasing NO₂ exposures, nitrites are gradually converted into nitrates.^{15,19}

Figure 1a presents the TPD profiles recorded after 900 L (5×10^{-7} Torr \times 30 min, $1 \text{ L} = 10^{-6}$ Torr \times s) NO₂ exposure (i.e., saturation) on a freshly prepared BaO_x(10 MLE)/Pt(111) model catalyst surface at 323 K. Two different NO desorption features at 620 and 670 K can be discerned in Figure 1a, corresponding to a two-stage nitrate decomposition mechanism as discussed in detail in our former reports.^{17,18} The first stage of the nitrate decomposition mechanism associated with the 620 K desorption feature reveals only NO desorption without any noticeable O₂ desorption signal. During this initial stage of nitrate decomposition, the produced oxygen species oxidize BaO domains to form BaO₂.^{17,18} BaO₂ formation process comes to a stop when peripheral BaO domains are saturated with oxygen. The second stage of the nitrate decomposition mechanism leads to a strong desorption peak at 670 K, revealing simultaneous desorption of NO and O₂. It is worth mentioning that discernible amounts of NO₂, N₂ or N₂O desorption were not observed in these set of TPD experiments. The broad O₂ ($m/z = 32$) desorption tail in Figure 1, extending toward 700–900 K, is attributed to the partial decomposition of BaO₂ at elevated temperatures.¹⁷

Figure 1b presents TPD spectra acquired after 900 L CO₂ adsorption ($P_{\text{CO}_2} = 5 \times 10^{-7}$ Torr, 30 min) on a thick BaO_x overlayer at 323 K, which was initially saturated with 1800 L NO₂ ($P_{\text{NO}_2} = 10^{-6}$ Torr, 30 min) at the same temperature.

TPD profiles given in Figure 1b are practically identical to that of Figure 1a. The concurrence of spectra in Figure 1a,b demonstrates the inability of the nitrated BaO_x overlayer to interact with CO₂. Apparently, the fully nitrated BaO_x surface does not reveal available adsorption sites for CO₂, and nitrates cannot be substituted with carbonates under these experimental conditions.

It is well-known that clean BaO_x overlayers can react with CO₂, forming carbonate species.^{20,21} Therefore, in order to confirm that a clean BaO_x overlayer can readily interact with CO₂, we performed XPS analysis of a CO₂-saturated thick BaO_x overlayer, which demonstrated a typical C1s peak at 289.5 eV (data not shown) and an O1s shoulder at 531.5 eV, in agreement with the corresponding values reported for BaCO₃.²⁰ TPD spectra associated with the exposure of a thick BaO_x overlayer to 1800 L (10^{-6} Torr \times 30 min) CO₂ at 323 K are presented in Figure 2a. Carbonate species, which are formed upon CO₂ adsorption, decompose by yielding a strong CO₂ ($m/z = 44$) desorption peak at 780 K. This particular CO₂ desorption signal is also accompanied by a CO ($m/z = 28$) desorption signal (due to the fragmentation of CO₂ in the ionizer section of QMS), which is also located at 780 K with a line shape that is similar to that of CO₂. It is worth mentioning that TPD spectra acquired after lower CO₂ exposures (e.g., 900 L) also result in an integrated CO₂ desorption signal whose magnitude is close to that of Figure 2a, indicating the complete saturation of the surface upon 1800 L CO₂ exposure. The temperature of the CO₂ desorption peak in Figure 2a is in good agreement with data published by A. Tsami et al.,²⁰ where they have observed a CO₂ desorption peak at 773 K on the BaO/Cu(111) surface. Mudiyansele et al.²¹ observed two different CO₂ desorption features for the BaO/Pt(111) surface, a main peak at 748 K and a less intense second peak at 825 K. The main desorption peak at 748 K has been associated with the thermal decomposition of bulk-like barium carbonate species and the 825 K peak has been attributed to the decomposition of surface carbonate species. In accordance with these former reports, the presence of a slight high-temperature asymmetry in

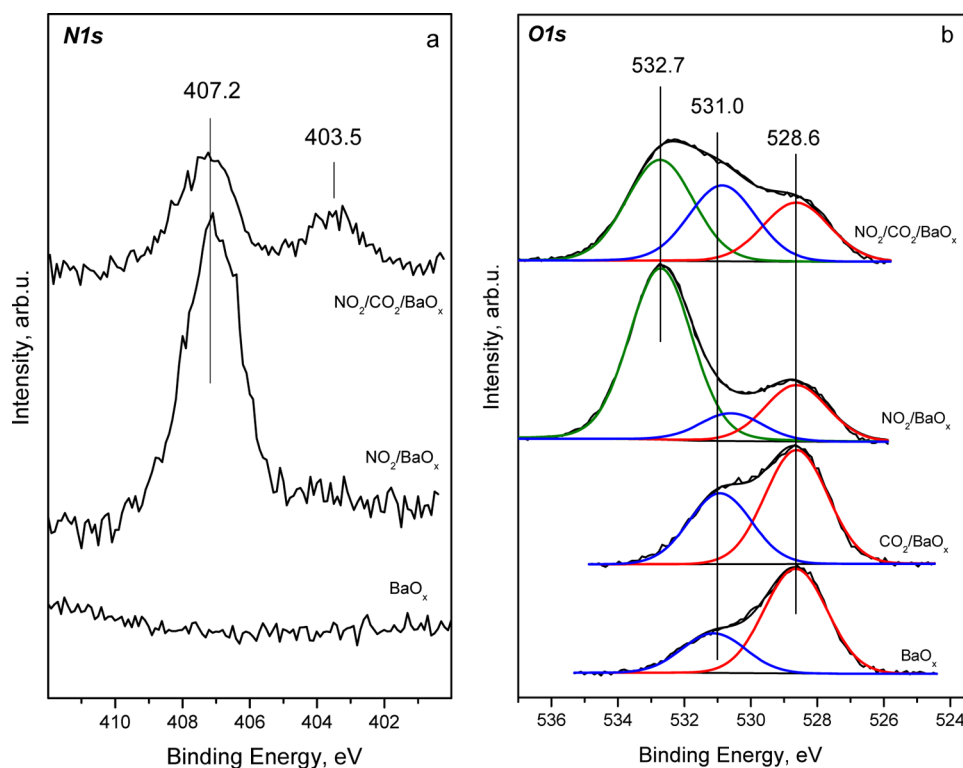


Figure 3. (a) N1s and b) O1s XP spectra obtained for clean, NO₂-saturated and CO₂-saturated BaO_x(>10 MLE)/Pt(111) surfaces as well as for an identical surface that was consequently saturated with first CO₂, then NO₂. All adsorption experiments were performed at 323 K.

the main CO₂ desorption signals in Figure 2a,b can be attributed to the decomposition of surface carbonates.

Figure 2b corresponds to the TPD spectra obtained after 1800 L NO₂ adsorption ($P_{\text{NO}_2} = 10^{-6}$ Torr \times 30 min) on a thick BaO_x/Pt(111) overlayer at 323 K, which was initially saturated with 1800 L CO₂ ($P_{\text{CO}_2} = 1 \times 10^{-6}$ Torr \times 30 min) at the same temperature. The presence of a strong NO ($m/z = 30$) desorption signal in Figure 2b demonstrates that CO₂-saturated BaO_x surface can readily interact with NO₂. The NO_x release is evident by the intense NO desorption peak at 615 K with a discernible shoulder at 670 K. Temperatures corresponding to these two NO desorption maxima are in very good agreement with the ones given in Figure 1a, and thus origins of these desorption features can be explained using a discussion that is analogous to the one given for Figure 1a, although a more comprehensive discussion can also be provided, as will be described later in the text. It is interesting to note that the second stage of the nitrate decomposition mechanism is suppressed in the presence of carbonates, which is consistent with the weak O₂ desorption (670 K) signal in Figure 2b, while the total integrated NO desorption signal is comparable to the data given in Figure 1a. It is clearly seen in Figure 2b that the NO_x desorption is completed at about 700 K. Above 700 K, that is after the completion of the NO_x desorption process, a new CO₂ desorption ($m/z = 44$) signal appears at 770 K, associated with the bulk carbonate decomposition. It is important to note that this particular $m/z = 44$ signal at 770 K cannot be assigned to N₂O, as this desorption feature is not accompanied by an NO ($m/z = 30$) signal at 770 K, as would be expected from an actual N₂O desorption feature.

The N1s XP spectra in Figure 3a belong to BaO_x(>10 MLE)/Pt(111) surfaces that are exposed to different conditions. The bottommost spectrum in Figure 3a corre-

sponds to the clean BaO_x(>10 MLE)/Pt(111) surface, which does not reveal any N1s features, as expected. The middle spectrum in Figure 3a was obtained after NO₂ saturation (900 L, $P_{\text{NO}_2} = 5 \times 10^{-7}$ Torr, 30 min) of a freshly prepared thick BaO_x overlayer yielding a strong N1s signal located at 407.2 eV due to nitrate species, as well as a very weak shoulder at \sim 404 eV originating from nitrites as the minority species.^{17,19,22} The topmost XP spectrum in Figure 3a corresponds to a NO₂-saturated (1500 L, $P_{\text{NO}_2} = 5 \times 10^{-7}$ Torr, 50 min) BaO_x(>10 MLE)/Pt(111) surface that was initially exposed to CO₂ (900 L, $P_{\text{CO}_2} = 5 \times 10^{-7}$ Torr, 30 min). Interestingly, this particular XP spectrum presents two clearly distinct N1s signals located at 407.4 and 403.5 eV that are associated with nitrates and nitrites, respectively. On the basis of the relative N1s XPS intensities, the nitrate:nitrite ratio for this surface is estimated to be 2:1. Observation of nitrites for the topmost spectrum suggests that the oxidation of NO_x to nitrates is hindered in the presence of carbonates. As described earlier in the text, it is likely that the formation of nitrate species involves an adsorbed NO₂ pair and the subsequent formation of a NO₂⁻ and NO₂⁺ couple,^{11–13} which are located on adjacent Lewis acid (Ba²⁺) and Lewis base (O²⁻) sites and formed through a disproportionation (intermolecular electron transfer) process. In other words, for the formation of nitrates, NO_x species require two adjacent unoccupied surface sites. It is well-known that CO₂ preferentially adsorbs on Lewis base (O²⁻) sites on BaO₉ making some of these sites unavailable for NO_x adsorption. Thus, due to the scarcity of the available Lewis base (O²⁻) sites on the precarbonated surface, NO₂ may preferably bind to Lewis acid (Ba²⁺) sites yielding nitrite species. Obviously, such a situation will increase the surface concentration of nitrites at the expense of nitrates.

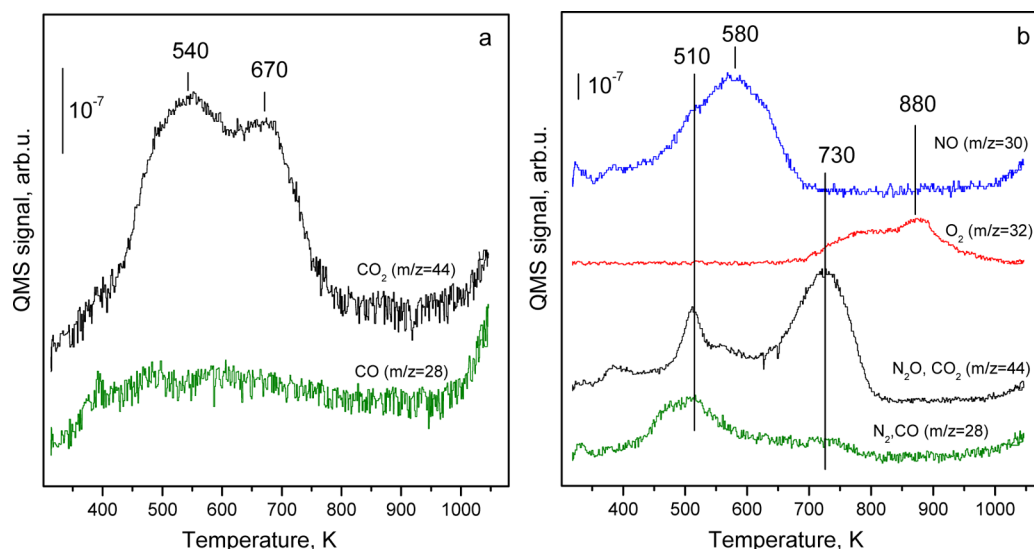
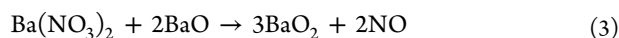


Figure 4. (a) TPD profiles showing the NO ($m/z = 30$), O₂ ($m/z = 32$), N₂/CO ($m/z = 28$), and N₂O/CO₂ ($m/z = 44$) desorption channels obtained after exposing a BaO_x(1.5 MLE)/Pt(111) surface to 900 L (5×10^{-7} Torr \times 30 min) CO₂(g) at 323 K. (b) TPD spectra obtained after consequent exposure of the BaO_x(1.5 MLE)/Pt(111) surface first to 900 L (5×10^{-7} Torr \times 30 min) CO₂(g), then to 900 L (5×10^{-7} Torr \times 30 min) NO₂(g).

The presence of nitrites on the precarbonated surface allows us to provide a detailed mechanistic explanation for the TPD data given in Figure 2b. Thus, the NO desorption signal at 615 K is associated with the decomposition of nitrates into nitrites, which is accompanied by the oxidation of BaO into BaO₂, followed by the decomposition of nitrites, which may also involve BaO₂ formation as described in the reactions given below:

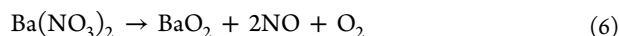
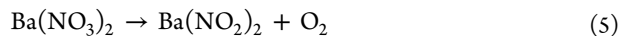


In addition, decomposition of nitrates without the formation of nitrites can also contribute to the 615 K desorption signal as shown in reaction 3,

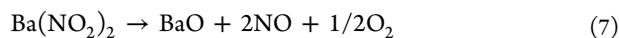


Apparently, due to the presence of carbonate species hindering the nitrate formation and favoring the presence of nitrites, reaction 2 presumably has a larger contribution to the 615 K desorption signal in Figure 2b, while such a contribution should be smaller for the 620 K signal in Figure 1a,b (i.e., in the absence of carbonates).

On the other hand, the 670 K desorption signal in Figure 2b, which is accompanied by O₂ release can be explained using the following reactions:



where nitrites formed at the second stage can further decompose according to reaction 2 or by yielding oxygen:



Finally, peroxides that are generated during the NO_x decomposition and release processes are decomposed partially at higher temperatures within 700–900 K to form BaO:



The O1s region of XP spectrum corresponding to a freshly prepared thick BaO_x overlayer is presented at the bottom of Figure 3b. In light of the former studies, the major O1s feature in this spectrum located at 528.6 eV can be attributed to BaO species;^{15,19} and the less intense feature at 531.0 eV can be assigned to BaO₂.^{17,23,24} BaCO₃ (carbonate) species reveal an O1s feature at 531–532 eV,^{24,25} which overlaps with the BaO₂ feature. After 900 L (5×10^{-7} Torr \times 30 min) CO₂ exposure on the BaO_x layer, the intensity of the 531.0 eV feature substantially increases (second spectrum from the bottom). The change in the intensity ratio of the 531.0 eV feature to that of the 528.6 eV feature confirms the carbonate formation on the BaO_x surface after CO₂ exposure, which is also evident by the presence of a typical C1s feature at 289.5 eV (data not shown). After NO₂ exposure on the clean BaO_x overlayer, the nitrate/nitrite related O1s feature appears at 532.7 eV. As expected, intensities of the O1s features corresponding to BaO (528.6 eV) and BaO₂ (531.0 eV) species decrease with increasing nitrate coverage. However, the relative intensities of these two peaks seem to stay rather unchanged. The uppermost spectrum in Figure 3 corresponds to NO₂ adsorption on a thick BaO_x overlayer, which was initially exposed to CO₂. The O1s XP spectrum for this surface reveals a BaO related feature at 528.6 eV, a BaO₂/BaCO₃ related feature at 531.0 eV, and a nitrate/nitrite related feature at 532.7 eV. In perfect agreement with the TPD results given in Figure 2b, XPS results given in Figure 3 also suggest that the carbonated BaO_x overlayer readily interacts with NO₂ to form nitrates/nitrites. XPS results given in Figure 3b also suggest that the intensity of the nitrate O1s feature for NO₂ adsorption on a CO₂ predosed surface is somewhat smaller than that of NO₂ adsorption on the clean surface. This is consistent with the previous experimental results on realistic NSR systems at elevated pressures reporting a decreased NSC in the presence of CO₂.^{5,8}

CO₂ and NO₂ Interactions on Small Two-/Three-Dimensional (2D/3D) BaO_x Clusters on Pt(111): Influence of Exposed Pt Sites. In order to elucidate the influence of exposed Pt sites on the CO₂–NO₂ surface chemistry, we exposed a BaO_x(1.5 MLE)/Pt(111) model catalyst to CO₂ 900

L (5×10^{-7} Torr \times 30 min). This surface will be referred to as the “thin BaO_x overlayer” hereafter in the text. TPD data obtained after such an exposure are given in Figure 4a. Our former studies suggest that at this coverage, the BaO_x overlayer is comprised of 2D islands and/or small 3D clusters.¹⁷ It is clear that the CO₂ desorption characteristics of thin BaO_x overlayer (Figure 4a) are significantly different than that of the thick BaO_x overlayer (Figure 2a). For the thin BaO_x overlayer and in the presence of exposed Pt sites, the CO₂ desorption signal appears at significantly lower temperatures in the form of two overlapping peaks at 540 and 670 K. Thus the low-temperature CO₂ desorption feature in Figure 4a at 540 K can be associated with the decomposition of carbonates in the vicinity of exposed Pt sites, while the 670 K feature can be associated with decomposition of carbonates from the terraces of 2D islands and/or 3D clusters, which are located farther from Pt sites. It is worth mentioning that a similar decrease in the thermal desorption maxima was also observed for NO₂ adsorption on thin BaO_x overlayers on Pt(111) where the presence of exposed Pt sites as well as the Pt/BaO_x interfacial sites was found to facilitate the nitrate decomposition.¹⁷

We also carried out experiments analogous to the ones given in Figure 1b, where we performed CO₂ adsorption on a nitrated thin BaO_x overlayer at 323 K. However, as in Figure 1b, CO₂ was not found to interact significantly with the nitrated thin BaO_x overlayer (data not shown).

Figure 4b shows TPD results obtained after NO₂ saturation 900 L (5×10^{-7} Torr \times 30 min) of a thin BaO_x overlayer at 323 K, which is initially saturated with CO₂ 900 L (5×10^{-7} Torr \times 30 min) at the same temperature. When the $m/z = 28$ desorption channel in Figure 4b is investigated, the broad desorption feature at \sim 500 K can be attributed to N₂ species, which are formed as a result of the recombinative desorption of atomic nitrogen (N_{ads}) species generated with the help of exposed Pt sites. A similar $m/z = 28$ feature at \sim 500 K was also reported in former studies for the NO₂ adsorption on a BaO_x/Pt(111) surface having exposed Pt sites.^{17,26}

In Figure 4b, the $m/z = 44$ desorption signal reveals a readily visible feature at 510 K that can be associated with N₂O desorption since it is accompanied by corresponding N₂ and NO desorption signals at the same temperature. On the other hand, it should be noted that a contribution to this $m/z = 44$ desorption signal from CO₂ species should not be excluded either. The main $m/z = 44$ desorption signal at 730 K can be readily assigned to CO₂ desorption (note that there is no NO desorption signal at this temperature, thus contribution to this peak from N₂O species can be ruled out). NO ($m/z = 30$) desorption from this surface appears as a broad peak at 580 K with a visible shoulder at 510 K. As described earlier, the latter (510 K) feature can be attributed mostly to N₂O as well as to Pt-assisted nitrate decomposition at the Pt/BaO_x interfacial/peripheral sites. The main NO desorption signal at 580 K as well as the CO₂ desorption signal at 730 K can be associated with nitrate/nitrite and carbonate decomposition from 3D BaO_x clusters, respectively. It should be noted that the carbonate decomposition temperature in Figure 4b is higher than the corresponding CO₂ desorption observed in Figure 4a. This behavior can be explained by adsorbate diffusion toward the subsurface region of the 2D/3D BaO_x domains upon sequential CO₂ and NO₂ adsorption. It is plausible that NO₂ adsorption on the carbonated surface imposes diffusion of the surface carbonates into the subsurface region of the 3D BaO_x clusters resulting in bulk-like carbonates that desorb at 770 K, a

temperature that is very close to carbonate desorption from thick BaO_x overlayers. Figure 4b also shows a relatively strong O₂ desorption signal yielding two discernible maxima at 775 and 880 K. The noticeable amount of O₂ evolution at high temperatures can be associated with the exposed Pt/BaO_x interfacial sites that are facilitating BaO₂ decomposition.

Influence of Thermal Aging and CO₂/NO₂ Adsorption on the Morphology of 2D/3D BaO_x Clusters. In order to shed light on the morphology changes inflicted on BaO_x domains upon thermal aging as well as nitration and carbonation, we performed surface Ba/Pt atomic ratio analysis on BaO_x(1.5 MLE)/Pt(111) model catalyst surfaces via XPS. As mentioned earlier, this BaO_x overlayer is considered to be mainly composed of 2D islands and/or small 3D clusters. Figure 5 demonstrates Ba/Pt surface atomic ratio changes for a

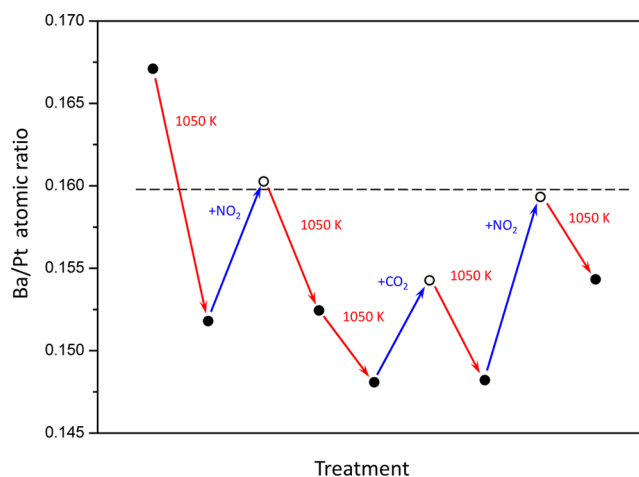


Figure 5. Ba/Pt surface atomic ratios corresponding to a BaO_x(1.5 MLE)/Pt(111) surface obtained after consecutive vacuum annealing, NO₂ saturation, and CO₂ saturation steps (all adsorption experiments were performed at 323 K).

BaO_x(1.5 MLE)/Pt(111) model catalyst surface that was treated with consecutive thermal aging (i.e., vacuum annealing between 323–1050 K with a temperature ramp of 1 K/s), nitration (i.e., NO₂ saturation at 323 K, 900 L), and carbonation (i.e., CO₂ saturation at 323 K, 900 L) protocols. For the Ba/Pt surface atomic ratio calculations, Ba3d and Pt4f XPS signals were utilized by taking the corresponding photoemission sensitivity factors into account.²⁷ It is visible in Figure 5 that all of the vacuum annealing steps result in a decrease in the Ba/Pt surface atomic ratio. This can be explained by sintering of the BaO_x domains to form bigger aggregates on the surface. Alternatively, such an observation can also originate from Ba/BaO_x desorption from the surface. It is worth mentioning that, in the literature, BaO desorption from a BaO/ θ -Al₂O₃/Ni(100) surface has been observed at 1055 K for small BaO coverages, and the desorption temperature has been found to increase with increasing BaO_x coverage.²⁸ We monitored Ba desorption via QMS during the vacuum annealing steps (by following doubly ionized Ba²⁺ signal at $m/z = 69$), however, no Ba desorption signal was observed under the current experimental conditions. Alternatively, such a decrease in the Ba/Pt surface atomic ratio upon annealing may be also attributed to the diffusion of Ba or BaO_x species into the underlying Pt(111) framework. In such a case, after the removal of the BaO_x overlayer with Ar⁺ ion sputtering

and annealing the Pt(111) surface to high temperatures, subsurface Ba/BaO_x species are expected to segregate on the surface and become visible via XPS. However, no such species were observed in XPS after Ar⁺ ion sputtering and annealing. Thus, the decrease in the Ba/Pt surface atomic ratio observed after annealing steps in Figure 5 is most likely due to sintering of BaO_x domains.

Interestingly, Figure 5 clearly shows that NO₂ or CO₂ adsorption has an exclusive effect on the Ba/Pt surface atomic ratio where the Ba/Pt ratio is observed to increase after the saturation of the surface with either NO₂ or CO₂. It should be noted that the inelastic mean free path of the photoelectrons emitted from Ba3d states (with a KE = 707 eV for Al K α source) ranges within 15.66–17.03 Å for BaO, Ba(NO₃)₂, and BaCO₃, where the longest inelastic mean free path belongs to BaO.²⁹ In other words, in the absence of any morphological alterations, nitration or carbonation of the BaO_x/Pt(111) overlayer is expected to decrease the Ba/Pt ratio. In stark contrast to this fact, Figure 5 indicates that the experimental Ba/Pt surface atomic ratio increases after each nitration or carbonation protocol in a consistent manner. A plausible explanation for the increase in the Ba/Pt surface atomic ratio upon nitration or carbonation could be a morphological modification in which nitration or carbonation imposes dispersion and spreading of the BaO_x domains on the Pt(111) substrate. These results clearly demonstrate the dynamic nature of the BaO_x overlayer morphology, which can readily be altered by the presence of common adsorbates such as NO₂ and CO₂.

CONCLUSIONS

In the current study, we focused our attention on the interactive surface chemistry of CO₂ and NO₂ on BaO_x/Pt(111) model catalyst surfaces with a particular emphasis on the competition between different adsorbates for the catalytic adsorption sites and adsorbate induced morphological changes. Some of our major findings can be summarized as follows:

- After NO₂ adsorption, nitrated BaO_x/Pt(111) surfaces do not reveal available adsorption sites for CO₂, irrespective of the presence/absence of exposed Pt sites on the surface.
- Although NO₂ adsorption on thick BaO_x/Pt(111) overlayers leads to the formation of predominantly nitrate species, NO₂ adsorption on the corresponding carbonated surface leads to the formation of coexisting nitrates and nitrites. The presence of carbonates on BaO_x/Pt(111) overlayers does not prevent NO₂ uptake.
- Carbonated thin BaO_x/Pt(111) surfaces obtained via CO₂ adsorption can further interact with NO₂, forming surface nitrate/nitrite species, accompanied by the transformation of surface carbonates into bulk carbonate species. These results are consistent with the need for two adjacent unoccupied adsorption sites for the nitrate formation process. It is apparent that in the presence of both NO₂ and CO₂, carbonate species formed on Lewis base (O²⁻) sites enable the formation of nitrites at Lewis acid (Ba²⁺) sites.
- Carbonates formed on clean and thick BaO_x overlayers decompose at ~780 K, while in the presence of exposed (uncovered) Pt sites, carbonate decomposition is facilitated by the Pt sites, and the carbonate decom-

position temperature decreases to significantly lower temperatures between 500–700 K.

- Thermal aging, nitration and carbonation have a direct influence on the morphology of the 2D/3D BaO_x aggregates on Pt(111). While thermal aging in vacuum leads to the sintering of the BaO_x domains, nitration and carbonation results in redispersion and spreading of the BaO_x domains on the Pt(111) substrate.

AUTHOR INFORMATION

Corresponding Author

*E-mail: ozensoy@fen.bilkent.edu.tr.

Notes

The authors declare no competing financial interest.

ACKNOWLEDGMENTS

E.O. acknowledges support from the Turkish Academy of Sciences (TUBA) through the “Outstanding Young Investigator” grant. E.I.V. and V.I.B. acknowledge RFBR (Russia) #12-03-91373-CT_a, for financial support. Financial support for this work was provided by the Scientific and Technical Research Council of Turkey (TUBITAK) (Project Code: 107Y115). Authors also gratefully acknowledge Prof. Mehmet Erbudak (ETH Zurich) for his invaluable assistance with the UHV experimental setup.

REFERENCES

- (1) Miyoshi, N.; Matsumoto, S.; Katoh, K.; Tanaka, T.; Harada, J.; Takahashi, N.; Yokota, K.; Sugiura, M.; Kasahara, K. Development of New Concept Three-Way Catalyst for Automotive Lean-Burn Engines. *SAE Int. Tech. Pap.* **1995**, DOI: 10.4271/950809.
- (2) Fekete, N.; Kemmler, R.; Voigtlander, D.; Krutzsch, B.; Zimmer, E.; Wenninger, G.; Strehlau, W.; van den Tillaart, J. A. A.; Leyrer, J.; Lox, E. S.; Muller, W. Evaluation of NO_x Storage Catalysts for Lean Burn Gasoline Fueled Passenger Cars. *SAE Int. Tech. Pap.* **1997**, DOI: 10.4271/970746.
- (3) Epling, W. S.; Campbell, L. E.; Yezerets, A.; Currier, N. W.; Parks, J. E., II Overview of the Fundamental Reactions and Degradation Mechanisms of NO_x Storage/Reduction Catalysts. *Catal. Rev.* **2004**, *46*, 163–245.
- (4) Liu, G.; Gao, P.-X. A Review of NO_x Storage/Reduction Catalysts: Mechanism, Materials and Degradation Studies. *Catal. Sci. Technol.* **2011**, *1*, 552–568.
- (5) Balcon, S.; Potvin, C.; Salin, L.; Tempere, J. F.; Djega-Mariadassou, G. Influence of CO₂ on Storage and Release of NO_x on Barium-Containing Catalyst. *Catal. Lett.* **1999**, *60*, 39–43.
- (6) Cant, N. W.; Patterson, M. J. The Storage of Nitrogen Oxides on Alumina-Supported Barium Oxide. *Catal. Today* **2002**, *73*, 271–278.
- (7) Hendershot, R. J.; Vijay, R.; Snively, C. M.; Lauterbach, J. High-Throughput Study of the Influence of H₂O and CO₂ on the Performance of Nitrogen Storage and Reduction (NSR) Catalysts. *Appl. Surf. Sci.* **2006**, *252*, 2588–2592.
- (8) Rodrigues, F.; Juste, L.; Potvin, C.; Tempere, J. F.; Blanchard, G.; Djega-Mariadassou, G. NO_x Storage on Barium-Containing Three-Way Catalyst in the Presence of CO₂. *Catal. Lett.* **2001**, *72*, 59–64.
- (9) Tutuianu, M.; Inderwildi, O. R.; Bessler, W. G.; Warnatz, J. Competitive Adsorption of NO, NO₂, CO₂, and H₂O on BaO(100): A Quantum Chemical Study. *J. Phys. Chem. B* **2006**, *110*, 17484–17492.
- (10) Broqvist, P.; Panas, I.; Gronbeck, H. Toward a Realistic Description of NO_x Storage in BaO: The Aspect of BaCO₃. *J. Phys. Chem. B* **2005**, *109*, 9613–9621.
- (11) Schneider, W. F. Qualitative Differences in the Adsorption Chemistry of Acidic (CO₂, SO_x) and Amphiphilic (NO_x) Species on the Alkaline Earth. Oxides. *J. Phys. Chem. B* **2004**, *108*, 273–282.

(12) Schneider, W. F.; Hass, K. C.; Miletic, M.; Gland, J. L. Dramatic Cooperative Effects in Adsorption of NO_x on MgO(001). *J. Phys. Chem. B* **2002**, *106*, 7405–7413.

(13) Gronbeck, H.; Broqvist, P.; Panas, I. Fundamental Aspects of NO_x Adsorption on BaO. *Surf. Sci.* **2006**, *600*, 403–408.

(14) Yi, C.-W.; Kwak, J. H.; Szanyi, J. Interaction of NO₂ with BaO: From Cooperative Adsorption to Ba(NO₃)₂ Formation. *J. Phys. Chem. C* **2007**, *111*, 15299–15305.

(15) Schmitz, P.; Baird, R. NO and NO₂ Adsorption on Barium Oxide: Model Study of the Trapping Stage of NO_x Conversion via Lean NO_x Traps. *J. Phys. Chem. B* **2002**, *106*, 4172–4180.

(16) Alexander, M. R.; Thompson, G. E.; Zhou, X.; Beamson, G.; Fairley, N. Quantification of Oxide Film Thickness at the Surface of Aluminium Using XPS. *Surf. Interface Anal.* **2002**, *34*, 485–489.

(17) Vovk, E. I.; Emmez, E.; Erbudak, M.; Bukhtiyarov, V. I.; Ozensoy, E. Role of the Exposed Pt Active Sites and BaO₂ Formation in NO_x Storage Reduction Systems: A Model Catalyst Study on BaO_x/Pt(111). *J. Phys. Chem. C* **2011**, *115*, 24256–24266.

(18) Emmez, E.; Vovk, E. I.; Erbudak, M.; Bukhtiyarov, V. I.; Ozensoy, E. Direct Evidence for the Instability and Deactivation of Mixed-Oxide Systems: Influence of Surface Segregation and Subsurface Diffusion. *J. Phys. Chem. C* **2011**, *115*, 22438–22443.

(19) Desikusumastuti, A.; Happel, M.; Dumbuya, K.; Staudt, T.; Laurin, M.; Gottfried, J. M.; Steinruck, H.-P.; Libuda, J. Modeling NO_x Storage Materials: On the Formation of Surface Nitrites and Nitrates and Their Identification by Vibrational Spectroscopy. *J. Phys. Chem. C* **2008**, *112*, 6477–6486.

(20) Tsami, A.; Grillo, F.; Bowker, M.; Nix, R. M. Model NSR Catalysts: Fabrication and Reactivity of Barium Oxide Layers on Cu(111). *Surf. Sci.* **2006**, *600*, 3403–3418.

(21) Mudiyansele, K.; Yi, C.-W.; Szanyi, J. Reactivity of a Thick BaO Film Supported on Pt(111): Adsorption and Reaction of NO₂, H₂O, and CO₂. *Langmuir* **2009**, *25*, 10820–10828.

(22) Ozensoy, E.; Peden, C. H. F.; Szanyi, J. Model NO_x Storage Systems: Storage Capacity and Thermal Aging of BaO/θ-Al₂O₃/NiAl(100). *J. Catal.* **2006**, *243*, 149–157.

(23) Yi, C.-W.; Kwak, J. H.; Szanyi, J. Interaction of NO₂ with BaO: From Cooperative Adsorption to Ba(NO₃)₂ Formation. *J. Phys. Chem. C* **2007**, *111*, 15299–15305.

(24) Bowker, M.; Cristofolini, M.; Hall, M.; Fourre, E.; Grillo, F.; McCormack, E.; Stone, P.; Ishii, M. NSR Catalysis Studied Using Scanning Tunneling Microscopy. *Top. Catal.* **2007**, *42*, 341–343.

(25) Gauzzi, A.; Mathieu, H. J.; James, J. H.; Kellett, B. AES, XPS and SIMS Characterization of YBa₂Cu₃O₇ Superconducting High T_c Thin Films. *Vacuum* **1990**, *41*, 870–874.

(26) Gland, J. L.; Sexton, B. A. Nitric Oxide Adsorption on the Pt(111) Surface. *Surf. Sci.* **1980**, *94*, 355–368.

(27) Scofield, J. H. Hartree–Slater Subshell Photoionization Cross-Sections at 1254 and 1487 eV. *J. Electron Spectrosc. Relat. Phenom.* **1976**, *8*, 129–137.

(28) Ozensoy, E.; Peden, C. H. F.; Szanyi, J. Ba Deposition and Oxidation on θ-Al₂O₃/NiAl(100) Ultrathin Films. Part II: O₂(g) Assisted Ba Oxidation. *J. Phys. Chem. B* **2006**, *110*, 17009–17014.

(29) Tanuma, S.; Powell, C. J.; Penn, D. R. Calculation of Electron Inelastic Mean Free Paths (IMFPs) VII. Reliability of the TPP-2M IMFP Predictive Equation. *Surf. Interface Anal.* **2003**, *35*, 268–275.